

ARTICLE

Received 29 Feb 2016 | Accepted 12 May 2016 | Published 17 Jun 2016

DOI: 10.1038/ncomms11915

OPEN

Early synaptic deficits in the APP/PS1 mouse model of Alzheimer's disease involve neuronal adenosine A_{2A} receptors

Silvia Viana da Silva^{1,2}, Matthias Georg Haber^{3,*}, Pei Zhang^{1,*}, Philipp Bethge¹, Cristina Lemos⁴, Nélío Gonçalves⁴, Adam Gorlewicz¹, Meryl Malezieux¹, Francisco Q. Gonçalves⁴, Noëlle Grosjean¹, Christophe Blanchet¹, Andreas Frick³, U Valentin Nägerl¹, Rodrigo A. Cunha^{4,5} & Christophe Mulle¹

Synaptic plasticity in the autoassociative network of recurrent connections among hippocampal CA3 pyramidal cells is thought to enable the storage of episodic memory. Impaired episodic memory is an early manifestation of cognitive deficits in Alzheimer's disease (AD). In the APP/PS1 mouse model of AD amyloidosis, we show that associative long-term synaptic potentiation (LTP) is abolished in CA3 pyramidal cells at an early stage. This is caused by activation of upregulated neuronal adenosine A_{2A} receptors (A_{2A}R) rather than by dysregulation of NMDAR signalling or altered dendritic spine morphology. Neutralization of A_{2A}R by acute pharmacological inhibition, or downregulation driven by shRNA interference in a single postsynaptic neuron restore associative CA3 LTP. Accordingly, treatment with A_{2A}R antagonists reverts one-trial memory deficits. These results provide mechanistic support to encourage testing the therapeutic efficacy of A_{2A}R antagonists in early AD patients.

¹Interdisciplinary Institute for Neuroscience, University of Bordeaux, CNRS UMR 5297, F-33000 Bordeaux, France. ²BEB PhD program CNC Coimbra, 3004-517 Coimbra, Portugal. ³University of Bordeaux, Neurocentre Magendie, INSERM U862, F-33000 Bordeaux, France. ⁴CNC-Center for Neuroscience and Cell Biology, University of Coimbra, 3004-517 Coimbra, Portugal. ⁵Faculty of Medicine, University of Coimbra, 3004-504 Coimbra, Portugal. * These authors contributed equally to this work. Correspondence and requests for materials should be addressed to C.M. (email: christophe.mulle@u-bordeaux.fr).

Loss of episodic hippocampal-dependent memory is the earliest clinical sign of Alzheimer's disease (AD), consistent with reduced activation of hippocampal regions during memory encoding tasks in patients with mild cognitive impairment¹. Synaptic loss is the best morphological correlate of cognitive impairment in early AD, rather than amyloid-beta plaques, tangle formation or neuronal loss². The CA3 subregion of the hippocampus encodes episodic memories, particularly at the earliest stage of acquisition, presumably by developing instant representations of a context³. The autoassociative network of recurrent connections among CA3 pyramidal cells (PCs) is thought to enable the storage of episodic memories through synaptic plasticity of these associative/commissural (A/C) inputs^{4,5}. In mouse models of AD, synaptic dysfunction has been mostly studied in the CA1 region or dentate gyrus with very few studies addressing deficits in CA3 (ref. 6). Long-term potentiation (LTP) of synaptic transmission at Schaffer collateral-CA1 synapses is generally impaired in mouse models of AD (refs 6,7). Whether synaptic plasticity is affected in the recurrent CA3 network in AD mouse models has not yet been addressed.

Dysregulation of NMDA receptors (NMDAR) has been proposed as a link between A β accumulation and disruption of LTP (ref. 8) although neuromodulation systems may also be impaired. Epidemiologic studies indicate that regular caffeine intake attenuates memory decline during aging⁹ and reduces the risk to develop AD (ref. 10). In animal models of AD, chronic caffeine intake prevents memory deterioration, an effect mimicked by the selective inhibition of A_{2A} receptors (A_{2A}R), which are a main target of caffeine¹¹. Conversely, the overactivation of hippocampal A_{2A}R is sufficient to disrupt memory performance¹². A_{2A}R are upregulated in cortical areas of AD patients¹³ including in the hippocampal formation¹⁴, but the mechanisms by which the blockade of A_{2A}R restores memory impairment are not understood. The impact of A_{2A}R may depend on the stage of progression of the disease, with a role for astrocytic A_{2A}R at late stages¹⁴. Here we provide evidence for early synaptic dysfunction in CA3 PCs in a mouse model of AD, and we explore the implication of NMDAR and A_{2A}R.

Results

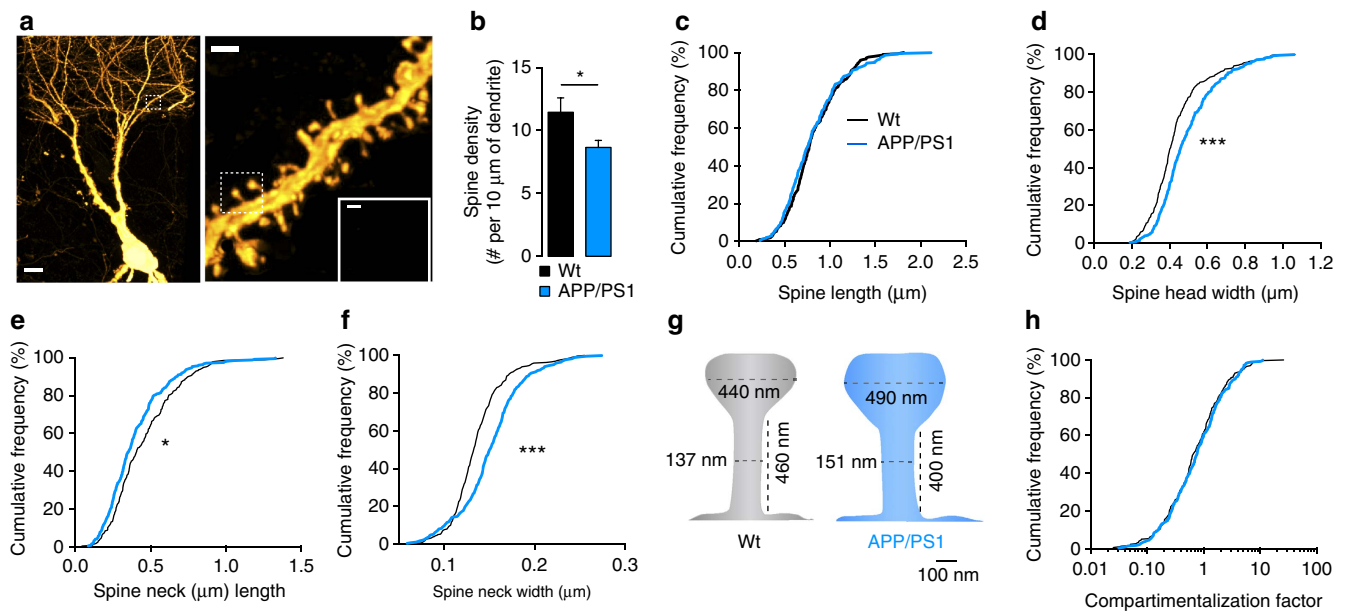
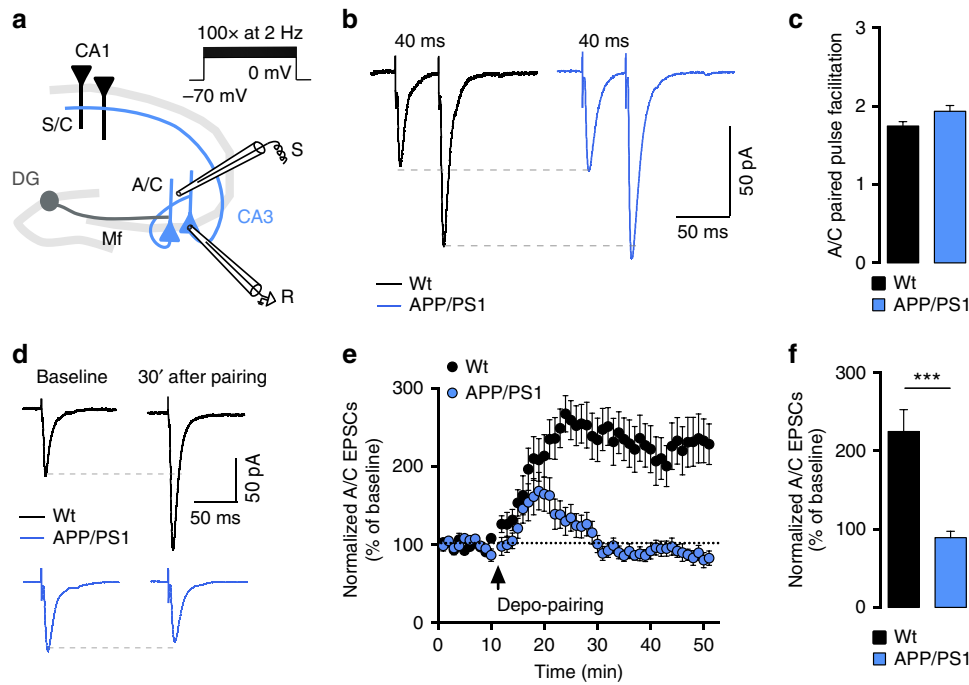
Impaired A/C synaptic plasticity in CA3 in APP/PS1 mice. We performed whole-cell patch clamp recordings of CA3 PCs to characterize the synaptic properties of A/C inputs in 6-month-old male APP/PS1 (Amyloid precursor protein (APP) gene with Swedish mutation and presenilin 1 gene (PS1) with deletion of exon 9) mice at early stages of amyloid-beta deposition¹⁵ when the CA3 region appears largely spared (Supplementary Fig. 1a). We initially recorded excitatory postsynaptic current (mEPSCs), which arise from the different types of glutamatergic synapses impinging on CA3 PCs. The average amplitude of mEPSCs was significantly decreased in APP/PS1 compared with wild-type (wt) mice (wt: 29 ± 2 pA, APP/PS1: 23 ± 1 pA, $P = 0.007$), whereas mEPSC frequency, measured by the inter event interval (IEI), was only minimally affected (wt: 0.7 ± 0.2 s, APP/PS1: 0.9 ± 0.1 s; Supplementary Fig. 2a,b). The decreased amplitude was mainly attributed to mEPSCs with amplitudes < 50 pA, suggesting that large amplitude mEPSCs arising from mossy fibre-CA3 synapses¹⁶ were not affected (Supplementary Fig. 2b). We further found that the paired-pulse ratio (PPR) of A/C synaptic responses was not different between APP/PS1 (1.9 ± 0.1) and wt mice (1.8 ± 0.1), arguing against presynaptic alterations (Fig. 1a–c). Pairing of presynaptic activation and postsynaptic depolarization induces an NMDAR-dependent

LTP of A/C inputs in CA3 PCs (ref. 17). Pairing A/C stimulation (100 stimuli at 2 Hz) with a depolarization to 0 mV (Fig. 1a) induced a robust LTP of AMPA-EPSCs in wt mice ($218 \pm 38\%$), which was absent in APP/PS1 mice ($93 \pm 12\%$, $P < 0.0001$; Fig. 1d–f).

To explore the mechanisms underlying the abolition of LTP of A/C inputs in APP/PS1 mice, we first tested whether this loss was correlated with morphological alterations of CA3 dendritic spines. Bilateral stereotaxic injections of retrograde rabies virus expressing green fluorescent protein (GFP; RABV)¹⁸ into CA1 were performed to specifically label CA3 PCs. We quantified spine density and morphology in these neurons using stimulated emission depletion (STED) microscopy. We found a decrease in the density of spines in the *stratum radiatum* of APP/PS1 mice (wt: 11.5 ± 1.1 spines per $10 \mu\text{m}$, APP/PS1: 8.7 ± 0.6 spines per $10 \mu\text{m}$, $P = 0.037$; Fig. 2a,b). STED microscopy allowed us to examine traditionally neglected key nanoscale features of spine morphology (Supplementary Table 2). Although spine length was similar in both genotypes (wt: $0.82 \pm 0.02 \mu\text{m}$, APP/PS1: $0.81 \pm 0.02 \mu\text{m}$, Fig. 2c), we found a marked shift to larger spine heads in APP/PS1 mice (wt: $0.44 \pm 0.01 \mu\text{m}$, APP/PS1: $0.49 \pm 0.01 \mu\text{m}$, $P < 0.0001$, Fig. 3d), in parallel with shorter and wider spine necks (Fig. 2e,f and Supplementary Table 2). As synapse compartmentalization is strongly shaped by spine morphology¹⁹, these changes (Fig. 2g) could potentially explain the decreased ability of the pairing protocol to induce LTP. However, the compartmentalization factor, which is a measure of biochemical compartmentalization of spine synapses (see definition in the Methods section), was preserved because the effects of the structural changes cancelled each other out (Fig. 2h). Thus the morphological phenotype seems insufficient to explain the absence of LTP observed at A/C synapses in APP/PS1 mice.

Loss of A/C LTP is not associated with alterations of NMDAR.

We tested whether dysregulation of NMDAR function, which has been implicated in impaired synaptic plasticity in models of AD (ref. 8), may be causally related to the loss of LTP in APP/PS1 mice. Insufficient membrane potential depolarization can be ruled out as a possible cause for the loss of A/C LTP in APP/PS1 mice as our LTP protocol controls for postsynaptic membrane potential. We found no difference in synaptic NMDAR/AMPA ratio between wt ($36 \pm 4\%$) and APP/PS1 mice ($37 \pm 5\%$; Fig. 3a,b). However, the relative expression of different GluN2 NMDAR subunits at synapses may strongly modulate plasticity²⁰, and the toxic effects of amyloid-beta oligomers applied in cultured neurons and acute slices is thought to involve the GluN2B subunit^{21,22}. We found no difference in the inhibition of NMDAR EPSC amplitude by Ro25-6981 ($1 \mu\text{M}$), a selective antagonist of GluN2B-containing NMDAR (wt: $59.0 \pm 5.9\%$, APP/PS1: $73.6 \pm 7.6\%$; Fig. 3c,d) or in NMDAR EPSC decay time (Supplementary Fig. 3a,b), ruling out a major change in GluN2 subunit composition of synaptic NMDAR in CA3 PCs in APP/PS1 mice. The subcellular localization of NMDAR (synaptic versus extrasynaptic) leads to the activation of different intracellular signalling pathways; importantly, extrasynaptic NMDAR were shown to be essential for amyloid-beta mediated toxicity^{23,24}. We evaluated extrasynaptic NMDAR by measuring the amplitude of tonic NMDAR-mediated currents recorded at $+40$ mV. Tonic currents were blocked to the same extent by the NMDAR antagonist D-AP5 ($50 \mu\text{M}$) in both genotypes (wt: 34 ± 4 pA and APP/PS1: 30 ± 5 pA; Fig. 3e,f). In addition, the blockade of tonic currents by Ro25-6981 ($1 \mu\text{M}$) did not indicate any change in GluN2B content (Supplementary Fig. 3c,d). Finally, we reasoned that if dysregulation of NMDAR was responsible for



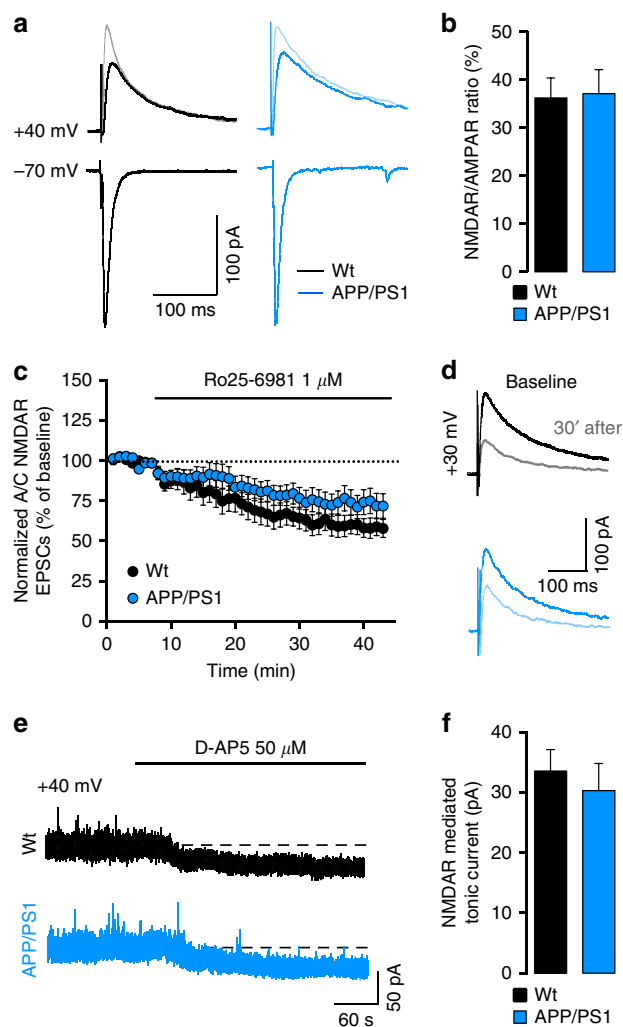


Figure 3 | Loss of A/C LTP is not associated with dysregulation of NMDAR. (a) A/C EPSCs were recorded at negative and positive potentials, and NMDAR-EPSCs were pharmacologically isolated with 20 μ M NBQX (darker traces at +40 mV). Traces represent the average of 40 sweeps recorded at 0.1 Hz. (b) Mean values of NMDAR/AMPA ratios obtained with isolated currents at -70 mV (AMPA) and +40 mV (NMDAR) from wt ($n=18$) and APP/PS1 mice ($n=16$; $P=0.894$, unpaired t -test). (c) Summary plot of the time course of A/C NMDAR-EPSCs amplitude during the application of Ro25-698 in wt ($n=13$) and APP/PS1 cells ($n=16$, $P=0.155$, unpaired t -test). Amplitude of A/C NMDAR-mediated EPSCs was normalized to the mean amplitude of an 8 min baseline period and quantification was performed after 30 min of drug application. (d) Average traces of pharmacologically isolated (20 μ M NBQX) A/C NMDAR-EPSCs obtained at a stimulation frequency of 0.1 Hz during baseline and after 30 min of Ro25-698 (1 μ M) application (lighter traces). (e) Representative examples of the shift in holding current observed in CA3 PCs clamped at +40 mV in response to D-AP5 revealing the tonic activation of extrasynaptic NMDAR at rest. AMPAR and KAR were blocked with 20 μ M NBQX. (f) Summarizing bar graph representing the shift of inward current in wt ($n=14$) and APP/PS1 cells ($n=14$, $P=0.573$, unpaired t -test). Data calculated as the difference between the last min of baseline and the last min after a 6-min D-AP5 application. Recordings were performed in the presence of 10 μ M bicuculline and 3 μ M CGP55845.

the loss of A/C LTP in APP/PS1 mice, then the selective potentiation of synaptic NMDAR by D-serine²⁵ may rescue plasticity. Enhancement of synaptic NMDAR by bath application of 10 μ M D-serine (~20% increase in current amplitude,

Supplementary Fig. 3e–g) did not rescue A/C LTP in APP/PS1 mice (109.0 \pm 9.5%, Supplementary Fig. 3h–j and Supplementary Table 1) or alter A/C LTP in wt mice. Hence, the complete loss of A/C LTP in 6-month-old APP/PS1 mice does not appear to correlate with alterations in the function or GluN2B content of neither synaptic nor extrasynaptic NMDAR.

Inhibition of A_{2A}R rescues A/C LTP in APP/PS1 mice. A_{2A}R control synaptic plasticity¹², are involved in memory impairment^{11,26} and are upregulated in the brain of AD patients^{13,14} and animal models of AD^{27,28}. We used a binding assay on isolated CA3 synaptic membranes and showed a robust increase of A_{2A}R density in 6-month-old APP/PS1 mice (wt: 38 \pm 7 fmol per mg protein; APP/PS1: 75 \pm 6 fmol per mg protein, $P=0.002$; Fig. 4a). Based on these results, we investigated if a short incubation of the slices for 10 min with the selective A_{2A}R antagonist SCH58261 (50 nM) could affect synaptic plasticity at A/C synapses. Strikingly, SCH58261 rescued in large part A/C LTP in APP/PS1 synapses (160 \pm 16%), in comparison with APP/PS1 slices treated with vehicle solution (98 \pm 9%, Fig. 4b–d). ZM241385 (50 nM), a chemically distinct and selective A_{2A}R antagonist was equally effective in rescuing A/C LTP (wt: 165.9 \pm 20.8%, $P=0.063$; Fig. 4d and Supplementary Table 1). The difference in mEPSCs amplitude observed between APP/PS1 and wt littermates (wt: 25.2 \pm 1.5 pA; APP/PS1: 19.5 \pm 1.1 pA) was not rescued by a short incubation with SCH58261 (wt_{SCH}: 24.0 \pm 1.5 pA; APP/PS1_{SCH}: 19.6 \pm 0.8 pA; $P=0.006$ for genotype effect; $P=0.173$ for drug effect, Supplementary Fig. 4a–c). Similarly, the distribution of mEPSCs amplitudes in both genotypes was not altered by SCH58261 (Supplementary Fig. 4b). Although SCH58261 incubation caused a small alteration in the distribution of IEIs between mEPSCs (Supplementary Fig. 4d), it did not cause any significant effect on the mean IEI values (wt_{Baseline}: 0.4 \pm 0.1 s; wt_{SCH58261}: 0.6 \pm 0.2 s; APP/PS1_{Baseline}: 0.6 \pm 0.2 s; APP/PS1_{SCH58261}: 0.8 \pm 0.2 s, Supplementary Fig. 4e).

A_{2A}R act synergistically with mGluR5 in hippocampal neurons²⁹, and mGluR5 antagonists rescue contextual fear conditioning in APP/PS1 mice³⁰. Accordingly, we found that a selective antagonist of mGluR5 (MTEP, 10 μ M) also rescued A/C LTP levels in APP/PS1 mice to values similar to those obtained with the A_{2A}R antagonist SCH58261 (164 \pm 28%, Fig. 5a–c). A combined incubation with both MTEP and SCH58261 did not further increase A/C LTP levels in 6-month-old APP/PS1 mice (163 \pm 18%, $P=0.008$, Fig. 5a–c and Supplementary Table 1), suggesting that A_{2A}R and mGluR5 operate through a common pathway to impair LTP. Importantly, these antagonists did not further increase the level of A/C LTP in wt mice (Supplementary Fig. 5a–c and Supplementary Table 1). Pharmacological inhibition of either A_{2A}R or mGluR5 did not fully rescue A/C LTP, possibly because the antagonists attenuate LTP in wt mice (Supplementary Fig. 4e,f). Adenosine neuromodulation depends on a balanced activation of inhibitory A₁R and A_{2A}R. We tested whether adenosine A₁R levels were comparatively affected by using a binding assay on purified CA3 synaptic membranes and observed a modest increase of A₁R density in 6-month-old APP/PS1 mice (wt: 938.2 \pm 27.2 fmol per mg protein; APP/PS1: 1044.0 \pm 19.0 fmol per mg protein, $P=0.002$; Supplementary Fig. 6a). To test if this alteration in A₁R density affected A/C synapses, we recorded evoked AMPAR EPSCs and bath applied 100 nM DCPCX (a selective A₁R antagonist). DCPCX equally increased the amplitude of AMPAR EPSCs in APP/PS1 (134.0 \pm 11.0%) and wt mice (143.3 \pm 17.8%, Supplementary Fig. 6b–d), arguing for similar levels of A₁R at those synapses.

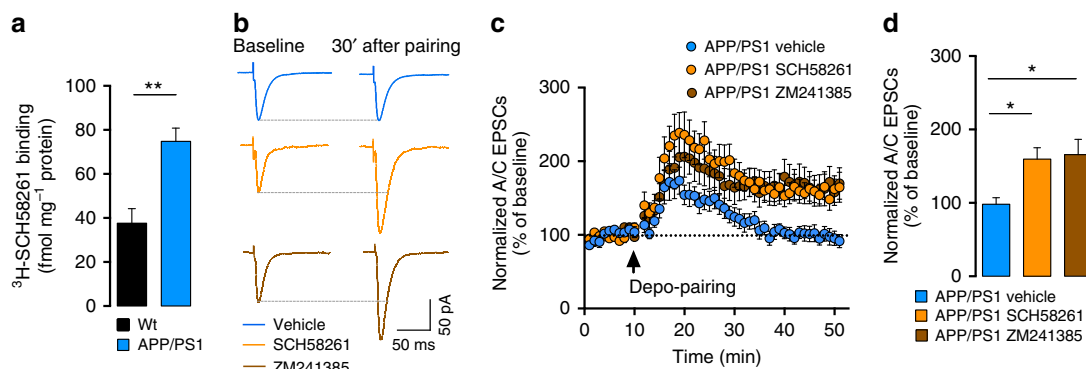


Figure 4 | Blockade of neuronal $A_{2A}R$ restores synaptic plasticity in CA3 PCs. (a) The density of $A_{2A}R$ is increased in synaptic membranes prepared from the CA3 region of APP/PS1 mice compared with wt littermates ($n = 6$, $**P = 0.002$, Mann-Whitney test). (b) Example traces representing a 10 min average of A/C-EPSCs before and 30 min after depo-pairing LTP protocol in the presence of SCH58261 (50 nM) or ZM241385 (50 nM). (c) Summary time course of normalized A/C-EPSCs recorded from APP/PS1 mice during LTP protocol performed in the presence of the two different $A_{2A}R$ antagonists or in control conditions. (d) Bar graph representing mean LTP amplitude recorded at 30–40 min after depo-pairing protocol represented in c. A 10-min incubation period with two different classes of $A_{2A}R$ antagonists, SCH58261 ($n = 11$) and ZM241385 ($n = 12$, $P = 0.006$ Kruskal-Wallis test with Dunn's multiple comparison test), rescued the LTP of A/C synapses in APP/PS1 mice ($n = 11$ for vehicle, Supplementary Table 1). Electrophysiology recordings were performed in the presence of 10 μM bicuculline and 3 μM CGP55845.

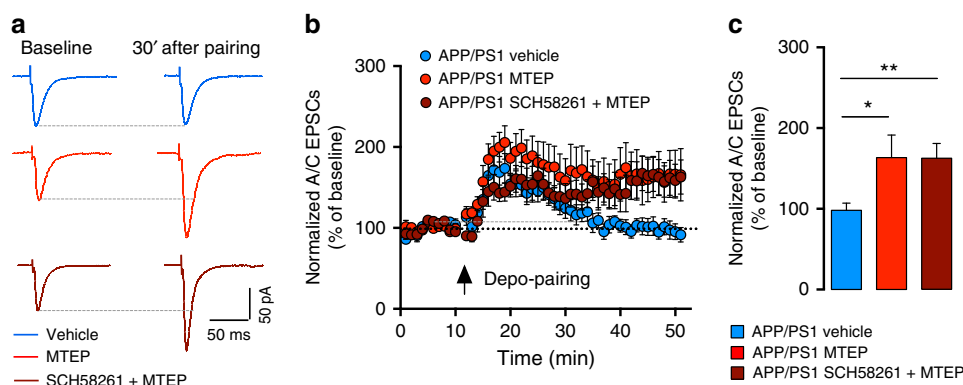


Figure 5 | $A_{2A}R$ and mGluR5 are involved in the loss of A/C LTP in APP/PS1 mice. (a) Example traces representing the average of A/C-EPSCs 10 min before and 30 min after depo-pairing LTP protocol. Recordings were performed in the presence of 10 μM bicuculline and 3 μM CGP55845. (b) Summary time course of normalized A/C-EPSCs recorded from APP/PS1 mice during LTP protocol performed in the presence of MTEP (10 μM) and MTEP + SCH58261 (50 nM). (c) Bar graph representing mean LTP amplitude recorded at 30–40 min after depo-pairing protocol represented in b. A 10-min incubation with MTEP ($n = 12$) or MTEP + SCH58261 ($n = 11$, $P = 0.008$ Kruskal-Wallis test with Dunn's multiple comparison test) rescued the LTP of A/C synapses in APP/PS1 mice ($n = 11$ for vehicle group, Supplementary Table 1).

$A_{2A}R$ antagonists can prevent $A\beta$ -induced memory impairment in mice²⁶. We thus tested whether SCH58261 (intraperitoneal injection, 0.1 mg per kg, for 6–7 days) could revert deficits in one-trial memory tasks, which depend on CA3 circuits^{3,4}, in a different group of 6-month-old APP/PS1 mice. When tested in the object displacement paradigm (30 min inter-trial interval), APP/PS1 mice showed impaired recognition of a displaced object, which was rescued on $A_{2A}R$ inhibition (Fig. 6a–c). Wt mice treated with saline displayed a higher displacement index ($68.2 \pm 4.0\%$), whereas APP/PS1 mice did not show any preference for the displaced object ($54.9 \pm 4.1\%$, $P = 0.034$ for genotype effect, Fig. 6b). This difference between genotypes was abrogated by SCH58261 treatment (wt_{SCH58261}: $63.5 \pm 3.3\%$; APP/PS1_{SCH58261}: $60.0 \pm 3.7\%$). Likewise, $A_{2A}R$ inhibition rescued the performance of APP/PS1 mice in a modified Y-maze task (30 min inter-trial interval), as shown by the increase in the percentage of time exploring the novel arm (wt_{Saline}: 40.5 ± 2.4 and APP/PS1_{Saline}: $34.6 \pm 2.8\%$, $P = 0.024$ for genotype effect, Fig. 6d–f). APP/PS1 mice treated with SCH58261 showed no difference in the time spent in the novel arm ($42.7 \pm 4.1\%$) when compared with wt mice treated with SCH58261 ($46.9 \pm 2.7\%$, Fig. 6e).

$A_{2A}R$ expressed in CA3 PCs are involved in A/C LTP deficits. Since both neuronal¹² and astrocytic $A_{2A}R$ (ref. 14) may control memory performance, we sought to understand if the pharmacological rescue of plasticity at early stages of AD is either due to an action on neurons or glia. For this purpose, we employed a knockdown approach of $A_{2A}R$ in neurons using a VSV-G-coated lentivirus expressing shRNA against $A_{2A}R$ and a fluorescent marker (sh $A_{2A}R$, see validation in Supplementary Information). One month after stereotaxic infection in the CA3 region of 5-month-old APP/PS1 mice, a few GFP-positive CA3 PCs (sh $A_{2A}R$ ⁺, expressing the shRNA) could be identified in hippocampal slices (Fig. 7a). To check for neuronal tropism of the lentiviral construct, we injected eGFP-sh $A_{2A}R$ lentivirus in the CA3 region of wt mice and performed immunohistochemistry on hippocampal sections. We observed a near exclusive co-localization with the neuronal marker NeuN for virally injected eGFP-positive cells, whereas no co-localization was observed with the astrocytic marker glial fibrillary acidic protein (GFAP) (Supplementary Fig. 7).

We found that genetic silencing of $A_{2A}R$ in individual CA3 PCs rescued LTP of A/C synapses in these cells in 6-month-old APP/

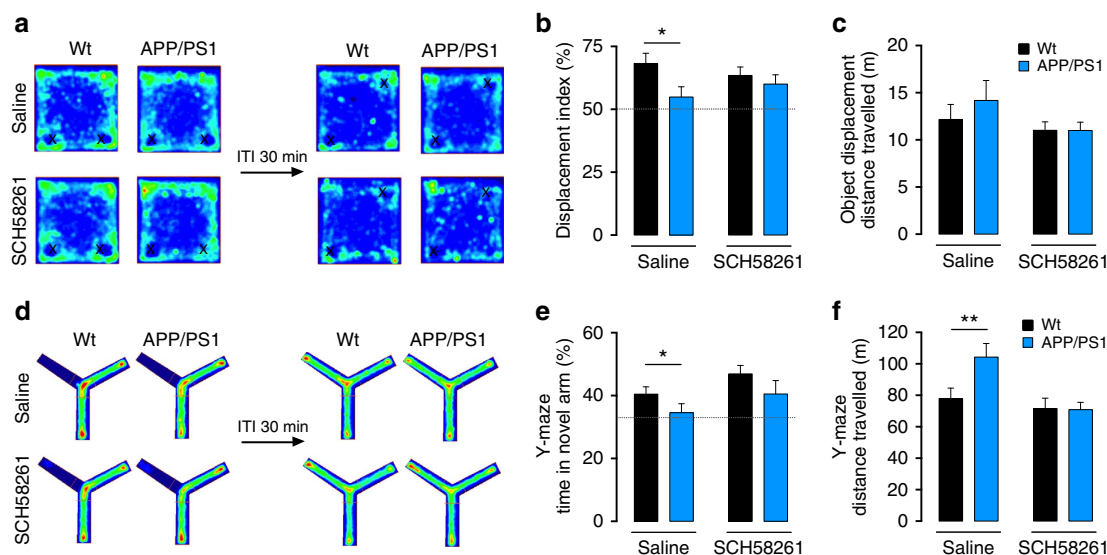


Figure 6 | Treatment with $A_{2A}R$ blockers restores one-trial memory impairment in APP/PS1 mice. (a) Average occupation plot representing the pattern of exploration of the mice in the object displacement test. Mice were treated with SCH58261 or saline for 6 days (b) Bar graph representing the percentage of time spent by mice exploring the displaced object. The displacement index is higher in $w_{t_{saline}}$ ($n = 12$) when compared with $APP/PS1_{saline}$ ($n = 9$, $*P = 0.034$, two-way ANOVA, genotype effect; Sidak's multiple comparisons test $w_{t_{saline}}$ versus $APP/PS1_{saline}$, $*P = 0.0374$). By contrast, whereas SCH58261 is devoid of effects in wt ($n = 11$, Sidak's multiple comparisons test $w_{t_{saline}}$ Saline versus $w_{t_{SCH58261}}$, $P = 0.594$), it reverted the lower percentage of time that APP/PS1 mice interacted with the novel object ($n = 10$, Sidak's multiple comparisons test $APP/PS1_{saline}$ versus $APP/PS1_{SCH58261}$, $P = 0.6047$). (c) No alterations were found in the average distance travelled by mice ($w_{t_{saline}}$: 12.2 ± 1.6 m, $n = 12$, $APP/PS1_{saline}$: 14.5 ± 1.9 m, $n = 9$, $P = 0.405$; $w_{t_{SCH58261}}$: 11.0 ± 0.9 m, $n = 11$, $APP/PS1_{SCH58261}$: 11.0 ± 0.9 m, $n = 10$, $P = 0.096$, two-way ANOVA). (d) Average occupation plot of exploration in the Y-maze task. (e) Bar graph representing the percentage of time spent in the novel arm by wt and APP/PS1 mice treated with SCH58261 or saline for 7 days. When comparing APP/PS1 ($n = 9$) and wt ($n = 12$) mice in the saline groups, we observed a difference in the percentage of time spent in the novel arm ($*P = 0.024$, two-way ANOVA, genotype effect; Sidak's multiple comparisons test $w_{t_{saline}}$ versus $w_{t_{SCH58261}}$, $*P = 0.0347$). SCH58261 treatment had no effect in wt groups ($n = 11$, Sidak's multiple comparisons test $w_{t_{saline}}$ versus $w_{t_{SCH58261}}$, $P = 0.901$), but reverted the memory deficit in APP/PS1 mice ($n = 10$, Sidak's multiple comparisons test $APP/PS1_{saline}$ versus $APP/PS1_{SCH58261}$, $P = 0.410$) (f) Distance travelled in the test phase of the modified Y-maze ($w_{t_{saline}}$: 77.9 ± 6.7 m, $n = 12$, $APP/PS1_{saline}$: 104.2 ± 8.6 m, $n = 9$; $w_{t_{SCH58261}}$: 71.5 ± 6.7 m, $n = 11$, $APP/PS1_{SCH58261}$: 70.8 ± 4.8 m, $n = 10$, $**P = 0.006$, two-way ANOVA with Sidak's multiple comparisons test). Horizontal dashed lines in b and e represent the random displacement values for better visualization.

PS1 mice. LTP of A/C synapses did not recover in uninfected neighbouring $sh-A_{2A}R^-$ CA3 PCs ($shA_{2A}R^+$: $174 \pm 20\%$, $shA_{2A}R^-$ cells: $92 \pm 9\%$, $P = 0.001$; Fig. 7a–c) or in cells infected with scramble RNA ($scrRNA^+$: $105 \pm 8\%$, Fig. 7d–f). A/C LTP could be rescued in $scrRNA^+$ cells with a short SCH58261 incubation as in control APP/PS1 CA3 PCs ($168 \pm 6\%$, $P = 0.0014$, Fig. 7d–f). Furthermore, the extent of A/C LTP following SCH58261 incubation was not different between $scrRNA^+$ and $shRNA^+$ cells ($173 \pm 15\%$), indicating that the $A_{2A}R$ shRNA occludes the effect of SCH58261 in $shRNA^+$ cells and not in control neurons (Supplementary Table 1 and Fig. 7f). This strongly suggests that the loss of A/C LTP is caused by gain of function of $A_{2A}R$ specifically in neurons and not glial cells at this early stage of AD. In addition, removal of $A_{2A}R$ from a single postsynaptic CA3 PC is sufficient to rescue A/C LTP, strongly suggesting a pathological function of postsynaptic $A_{2A}R$.

Discussion

This study provides the first characterization of AD-related synaptic impairment in the autoassociative network of recurrent connections between CA3 PCs which is crucially involved in the initial encoding of memory^{3,5}. At early stages of AD pathology in APP/PS1 mice, we found no major alteration of basal AMPAR or NMDAR-mediated transmission. However, we show that associative pairing between presynaptic A/C stimulation and postsynaptic spiking failed to induce LTP in single CA3 PCs.

Studies of LTP in mouse models of AD have often provided contradictory results⁶, possibly depending on the age and on the

experimental conditions to induce plasticity. In CA1, LTP of field EPSPs induced by high-frequency stimulation is attenuated—but not abolished—in an age-dependent manner in 4–6-month-old APP/PS1 mice³¹. Spine shape may determine the ability of synapses to undergo LTP by tuning biochemical and electrophysiological compartmentalization¹⁹. We observed a moderate decrease of spine density, which may correlate with subtle differences in the frequency of mEPSCs but cannot explain the abolition of LTP. Using STED microscopy, we unravelled subtle changes in spine necks and spine heads in 6-month-old APP/PS1 mice. However, as the morphological changes are predicted to leave biochemical synapse compartmentalization intact, it is unlikely that differences in synapse morphology can account for the LTP defect in APP/PS1 mice.

Associative LTP of A/C synapses depends on the activation of NMDAR during the induction phase^{17,32}. Many studies have proposed NMDAR and in particular GluN2B-containing NMDAR as targets for A β peptides⁸. GluN2B is thought to be important for induction of LTP, due to the direct physical interaction of its C-terminal tail with CaMKII (ref. 33). Our electrophysiological results indicate that the loss of A/C LTP in APP/PS1 mice cannot be attributed to decreased function of synaptic NMDAR or to a major change of GluN2B-containing NMDAR. We found no change in tonically activated extrasynaptic NMDAR, which were proposed to participate in the inhibition of LTP by soluble A β oligomers²³. In line with our data, chronic blockade of GluN2B-containing NMDAR does not rescue behaviour or spine morphology in PS2APP mice³⁴. We do not exclude the possibility that NMDAR

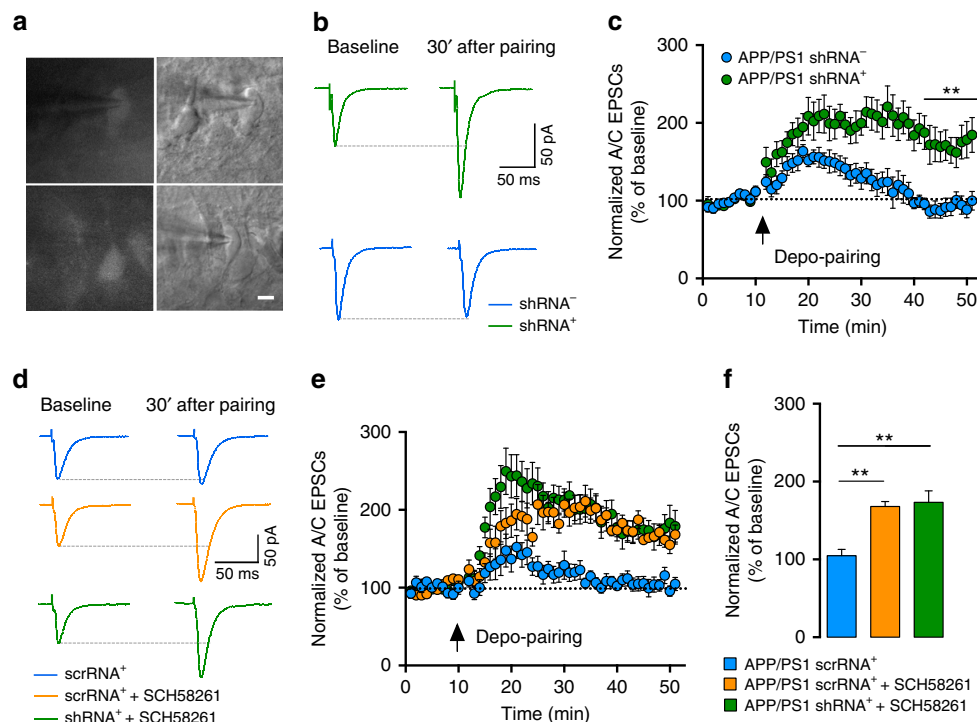


Figure 7 | Genetic silencing of neuronal $A_{2A}R$ restores A/C LTP. (a) Example pictures of CA3 PCs infected with shRNA lentivirus. Infected cells (shRNA⁺) and non-infected cells (shRNA⁻) in the proximity of infected cells were patched for the experiments in (b). Scale bar represents 10 μ m. (b) Example traces representing average A/C-EPSCs 10 min before and 30 min after LTP protocol in infected and non-infected cells. (c) Summary time course of normalized A/C-EPSCs during depo-pairing LTP protocol, recorded from APP/PS1 mice injected with $A_{2A}R$ shRNA; in shRNA⁺ cells there was a rescue of the A/C LTP ($n=7$) that was absent in shRNA⁻ cells ($n=7$, $**P=0.001$, Mann-Whitney test, Supplementary Table 1). (d) Example traces representing the average of A/C-EPSCs 10 min before and 30 min after depo-pairing LTP protocol in infected cells with $A_{2A}R$ shRNA or scrRNA lentivirus. (e) Summary time course of normalized A/C-EPSCs recorded from APP/PS1 mice during LTP protocol performed in scrRNA⁺ cells ($n=9$) in the absence and scrRNA⁺ ($n=7$) or shRNA⁺ cells ($n=9$) in the presence of SCH58261 (50 nM). (f) Bar graph representing mean LTP amplitude recorded at 30–40 min after depo-pairing protocol represented in e. APP/PS1 cells infected with scrRNA virus (scrRNA⁺) do not sustain LTP (Supplementary Table 1). A 10-min incubation period with SCH58261 increased LTP amplitude of scrRNA⁺ cells to levels similar to the genetic silencing of $A_{2A}R$ (Supplementary Table 1). In shRNA⁺ cells, SCH58261 did not further increase the LTP levels ($**P=0.0014$, Kruskal-Wallis test with Dunn's multiple comparison test between groups). All electrophysiology recordings were performed in the presence of 10 μ M bicuculline and 3 μ M CGP55845.

signalling may be strongly compromised at later stages of AD. However our study suggests that NMDAR may not be a valid target to restore hippocampal synaptic plasticity and the moderate cognitive deficits at early stage of AD pathology, in support of the lack of clinical efficiency of memantine in mild AD (ref. 35).

Strikingly, we found that the acute inhibition of $A_{2A}R$ by two different antagonists rescued LTP of A/C synapses, strongly suggesting that activation of $A_{2A}R$ by ambient adenosine or by adenosine produced during the LTP induction protocol disrupts synaptic plasticity in APP/PS1 mice. This raises several questions with regards to the source of adenosine, the cellular localization of $A_{2A}R$ and the signalling mechanism engaged to compromise LTP. On brain injury, $A_{2A}R$ undergo increased expression in both neurons and glia^{14,36}; their conditional removal from astrocytes ameliorates spatial memory selectively at later stages of AD (ref. 14). Our pharmacological experiments do not allow distinguishing effects of the antagonists on glial cells, pyramidal neurons or interneurons. However, we found that $A_{2A}R$ are upregulated in CA3 synapses at early stages of AD. Moreover, silencing $A_{2A}R$ selectively in an individual CA3 PC is sufficient to restore A/C LTP. Thus, the increase of $A_{2A}R$ in postsynaptic CA3 PCs can by itself explain the abolition of LTP. Although we cannot rule out an increased expression of astrocytic $A_{2A}R$ at this stage, this is not required for impaired plasticity. Interestingly, the

prevention of synaptic plasticity can be relieved by acute antagonism of $A_{2A}R$, providing some potential therapeutic strategies for early cognitive dysfunction in AD. Accordingly, the treatment of APP/PS1 mice with SCH58261 improved their one-trial spatial memory performance in both an object displacement and a modified Y-maze task, which is thought to depend on the activity of CA3 circuits³. More work is necessary to establish clear links between impaired A/C LTP and rapid acquisition of memory. Systemic administration of SCH58261 did not affect recall in one-trial memory tasks in wt mice, although it partly inhibited A/C LTP. Conversely, in APP/PS1 mice, behavioural deficits were markedly improved by SCH58261 administration, although A/C LTP deficit was only partly reverted.

The mechanism by which activation of upregulated $A_{2A}R$ compromises LTP is unknown. Because silencing $A_{2A}R$ in an individual CA3 PC rescues LTP, postsynaptic $A_{2A}R$ are likely at play. $A_{2A}R$ are pleiotropic receptors activating multiple G proteins and transducing pathways; the extended C-terminal domain of $A_{2A}R$ engages several proteins other than those canonically involved in signalling by G-protein coupled receptors³⁷. Furthermore, the signalling pathways of upregulated $A_{2A}R$ in disease-like conditions may be altered³⁸. Which of these multiple transducing systems is associated with the control by $A_{2A}R$ of synaptic plasticity is still unknown.

The ability of both A_{2A}R and mGluR5 to disrupt A/C LTP is intriguing and may provide a clue to the underlying mechanism²⁹. Interestingly, A_{2A}R and mGluR5 are both also necessary for the expression of LTP of NMDARs in CA3 PCs (ref. 39). The molecular mechanisms by which the amount of A_{2A}R is increased at early stages in neurons and at later (neuroinflammatory) stages in astrocytes still remains to be deciphered, in view of the complexity of the A_{2A}R gene promoter⁴⁰. Upregulation of A_{2A}R at early stages may not be restricted to CA3 PCs and may include interneurons and interneuronal connections to regulate the overall excitability of CA3 circuits⁴¹. Nevertheless, postsynaptic A_{2A}R in CA3 PCs, rather than such possible alterations account for deficits in A/C CA3 LTP.

Overall, the present study shows that at the early onset of AD-like features in APP/PS1 mice, associative long-term synaptic plasticity is abolished in CA3 PCs due to the activation of upregulated A_{2A}R in the postsynaptic compartment rather than to modifications of synaptic structure or NMDAR function. Our results are based on one-mouse model of AD, and it would certainly be important in the near future to extend this to other experimental models of cognitive deficits. Nonetheless, the exquisite ability of A_{2A}R blockade to restore the defective A/C CA3 LTP in APP/PS1 mice, in parallel to studies linking A_{2A}R to cognitive deficits^{11,12}, provides an additional mechanistic support to encourage testing the therapeutic efficacy of A_{2A}R antagonists in early AD patients.

Methods

Mice. APP/PS1 mice were obtained from Jackson's Lab and used according to regulations of the University of Bordeaux/CNRS Animal Care and Use Committee. The colony was maintained in a hemizygote state by crossing transgenic female mice to B6C3F1/J male mice. Throughout all their life, littermate wt and APP/PS1 male mice were housed in groups ranging from 4 to 10 animals per cage with free access to water and food. The large transparent plexiglas cages were kept in a temperature-regulated room on a 12-h light/dark cycle, and protected from exterior pathogens by a filter. All experiments were performed in the light phase of the circadian cycle in 6 months APP/PS1 and age-matched wt littermates.

Electrophysiology. Mice were anaesthetized with a ketamine (75 mg kg⁻¹) and xylazine (10 mg kg⁻¹) mix and intracardially perfused with ice-cold oxygenated cutting solution composed of 200 mM of sucrose, 20 mM glucose, 0.4 mM CaCl₂, 8 mM MgCl₂, 2 mM KCl, 1.3 mM NaH₂PO₄, 26 mM NaHCO₃, 1.3 mM ascorbate, 0.4 mM pyruvate and 3 mM kynurenic acid (pH 7.3). When the solution coming out of the heart was free of blood, mice were decapitated and the head immersed in ice-cold cutting buffer. The brain was quickly dissected and parasagittal slices (350 μm thick) were cut using a Leica vibratome (Leica VT 1200S) in the same solution. The slices were kept for 20 min in an oxygenated resting artificial cerebrospinal fluid (aCSF) containing 110 mM NaCl, 2.5 mM KCl, 0.8 mM CaCl₂, 8 mM MgCl₂, 1.25 mM NaH₂PO₄, 26 mM NaHCO₃, 0.4 mM ascorbate, 3 mM pyruvate and 14 mM glucose (pH 7.3) at 33 °C in the presence of kynurenic acid (2 mM). The slices were then transferred into another resting aCSF, now without kynurenic acid and left at room temperature for a maximum of 6 h after cutting. All drugs from Sigma-Aldrich, unless otherwise stated (see Supplementary Table 3 for details).

Cells were identified by differential interference contrast microscopy using an Olympus fixed stage upright microscope (BX51WI) equipped with a × 40 magnification immersion objective. Once at the electrophysiology set-up, slices were superfused with oxygenated (95% O₂, 5% CO₂) aCSF composed by 125 mM NaCl, 2.5 mM KCl, 2.3 mM CaCl₂, 1.3 mM MgCl₂, 1.25 mM NaH₂PO₄, 26 mM NaHCO₃ and 14 mM glucose (pH 7.4) and with 10 μM bicuculline. A period of 10 min was allowed for slice stabilization and removal of the excess Mg²⁺ from the resting solution. Whole-cell recordings were made at room temperature from visually identified CA3 PCs with borosilicate glass capillaries with 3–5 MΩ resistance filled with 140 mM CsMSO₃, 2 mM MgCl₂, 4 mM NaCl, 0.2 mM EGTA, 5 mM phosphocreatine, 3 mM ATPNa₂, 0.4 mM GTP and 10 mM HEPES (pH 7.2). The access resistance was < 20 MΩ and the experiment was discarded if it changed by > 20%. EPSCs were evoked using a patch pipette (~ 5 MΩ) filled with aCSF positioned in the CA3 stratum radiatum. The identification of the A/C synaptic currents was performed according to the following criteria: (1) frequency facilitation not > 1.2 when switching stimulation from 0.1 to 1 Hz, (2) paired-pulse facilitation ratio < 3 and (3) EPSCs decays free of a secondary peak that might indicate the presence of polysynaptic contamination. No liquid-junction potential correction was used. Recordings were made using an EPC10.0 amplifier (HEKA

Elektronik), filtered at 0.5–1 kHz and analysed using IGOR Pro and Neuromatic V2.6 softwares.

Stereotaxic injections and viral vectors. A small hairpin (sh) RNA was engineered to target the mouse A_{2A}R (shA_{2A}RNA), with the following sequence: 5'-CTA GTT TCC AAA AAG AAC TGC AGT CAG AAA TCT CTT GAA TTT CTG ACT GCA GTT GTT-3' and 5'-CGG GGA TCT GTG GTC TCA TAC AGA AC-3'. These oligomers and the H1 forward primer 5'-CAC CGA ACG CTG ACG TCA TCA ACC CG-3' were used for PCR with the pBC-H1 plasmid (pBC; Stratagene, Amsterdam, The Netherlands) containing the H1 promoter (GenBank: X16612, nucleotides 146–366) as a template. The silencing H1-shRNA cassettes were inserted into the lentivector plasmid SIN-cPPT-PGK-EGFP-WHV-LTR-TRE-RFA together with an EGFP reporter gene. As a control, we engineered a lentivector expressing a scrambled sequence of the RNA targeting A_{2A}R (scrRNA). Both the shA_{2A}RNA and scrRNA were packaged in VSV-G-coated lentiviral vectors. Lentivectors were produced in HEK293T cells, with a four-plasmid system, as previously described⁴² and the lentiviral particles content was determined by assessing HIV-1 p24 antigen levels (Gentaur, Spain). Viral stocks were stored at -80 °C until use and were thawed on ice before their *in vivo* administration. For control experiments, the lentivectors were administered to mice anaesthetized with avertin (240 μg g⁻¹, i.p.) and placed in a stereotaxic frame (Stoelting, Wood Dale, USA). To test the *in vivo* efficiency of the shA_{2A}RNA, we first injected the lentivector (286,000 ng of p24 antigen per ml) unilaterally into the mouse striatum, where the high density of A_{2A}R allows a faithful quantification of A_{2A}R downregulation. Mice received 1.4 μl of shA_{2A}RNA or scrRNA (0.2 μl per min) with an automatic injector (Stoelting) in the following coordinates: antero-posterior: +0.6 mm; medio-lateral: ± 1.8 mm; and ventral: -3.3 mm. After 3 weeks, an immunohistochemical analysis of the percentage striatal area labelled with eGFP (ref. 43) showed that the lentivectors transfected 27.2 ± 2.7% (n = 4) of the volume of dorsal striatum. This caused a 68 ± 8% (n = 4) decrease of A_{2A}R mRNA expression, evaluated by quantitative PCR (ref. 44) and a 55 ± 6% (n = 4) decrease of A_{2A}R protein density in the striatum, as evaluated by Western blot analysis⁴⁵. Mice were kept in their home cages for 4 weeks before being killed for preparation of slices and recording of transfected and non-transfected neurons, identified by the presence or absence of eGFP. The estimated amount of cells transfected varied from experiments to experiments and was ~ 15 cells per slice and 600 cells per infection (similar profile to Supplementary Fig. 6).

The GFP expressing RABV were stereotaxically injected as previously described⁴⁶ in CA1 stratum radiatum and the cellular CA3 morphology was analysed after 6 days. For STED microscopy, we performed immunohistochemistry (anti-GFP Alexa 488) on 60 μm brain sections to further increase the signal to background ratio.

Immunohistochemistry. (a) For immunolabelling performed on RABV infected brains, coronal sections (60 μm) were washed three times with 0.5% Triton-X100 (TX) in 1 × PBS (20 min each) and pre-incubated 1 h in a serum solution (goat serum 10% + 0.5% TX in 1 × PBS). The sections were washed three times with 1 × PBS and immersed in the primary antibody solution (rabbit anti-GFP antibody A11122, Invitrogen; 1/1,000 in 0.5% TX in 1 × PBS) for 24 h at 4 °C on a shaker. After washing four times with 1 × PBS, the sections were incubated with the secondary antibody (goat anti-rabbit Alexa Fluor 488 antibody, A11008 from Invitrogen; 1/1,000 diluted in 1 × PBS + 0.5% TX) for 2 h at room temperature. The brain sections were mounted in ProLong Gold Antifade mounting medium (Invitrogen/Molecular Probes) and covered by individual round glass coverslips of 18-mm diameter (0.17 ± 0.01 mm thick). (b) Immunolabelling for detection of amyloid plaques was performed as described above, using a primary antibody raised against human amyloid-beta peptides (polyclonal rabbit antibody, 1/500; ABCAM ab2539) and goat anti-rabbit secondary antibody coupled with Alexa Fluor 488. (c) Immunohistochemistry to determine the cell types infected in the hippocampal CA3 area was performed on sections from lentivirus infected mice as described above, using following antibodies: anti-NeuN (mouse Millipore MAB377, 1/400), anti-GFAP (rabbit Millipore AB5804, 1/1,000), donkey anti-mouse secondary antibody coupled Alexa Fluor 594 (1/200) and donkey anti-rabbit secondary antibody coupled Alexa Fluor 594 (1:200).

STED microscopy and morphometric analysis. Super-resolved images of spine morphology were obtained with a custom-built STED microscope with a nominal spatial resolution of 50 nm. All images were acquired in the stratum radiatum above the CA3b region as stacks of 10 z-sections with a step size of 192 nm and a pixel size of 40 nm × 40 nm. For spine counts and density calculations over large field-of-views (image from Fig. 2a left and data Fig. 2b), a home-built two-photon microscope (λ_{exc} = 920 nm) equipped with a water-immersion objective (60X LUMFI, 1.1 NA, Olympus) was used as previously described⁴⁷. For more detailed analyses of spine morphology we used a home-built STED microscope. It was based on an inverted microscope (DMI 6000 CS Trino, Leica), using a pulsed-laser diode (PDL 800-D, Picoquant) for excitation (λ_{exc} = 485 nm, ~ 90 ps) and a Ti:Sapphire system (Chameleon, Coherent; OPO, APE) for fluorescence quenching (λ_{STED} = 595 nm, ~ 200 ps), as described previously⁴⁸. The pulses of originally 200 fs duration were stretched to ~ 300 ps by dispersion via a 100-m-long

polarization-preserving fiber (Schäfer + Kirchhoff, Hamburg, Germany). To create the STED focal doughnut, a polymeric phase plate (RPC Photonics, Rochester, NY) was introduced into the path of the expanded STED beam, imprinting a helical phase ramp onto the wavefront. The STED and excitation pulses were synchronized via external triggering of the laser diode, and the delay was adjusted with a custom-built electronic delay generator. Both beams were overlapped with a dichroic mirror (AHF Analysentechnik, Tübingen, Germany), and focused onto the fixed sample by an oil objective (HCX PL APO, 1.47 NA, $\times 100$; Leica, Wetzlar, Germany). A telecentric beam scanner (Yanus IV, TILL Photonics, Gräfelfing, Germany) with scan and tube lenses from the microscope manufacturer was used to steer the beam. Focusing by the objective was controlled via a piezo actuator (P-721 PIFOC, PI Physik Instrumente, Karlsruhe, Germany). The fluorescence was collected episcopically using a dichroic mirror and a 525/50 band-pass filter, and imaged onto a multimode optical fiber connected to an avalanche photodiode (SPCM-AQR-13-FC, PerkinElmer, Waltham, MA). Images were acquired using ImSpector software (courtesy of A. Schönle, Max Planck Institute for Biophysical Chemistry, Göttingen, Germany). All morphological measurements were done using a custom-made plug-in for ImageJ where the spine length was measured from the base of the dendrite to the edge of the head, following the curvature of the spine neck. Spine neck width is reported as the average from multiple spine neck profiles, drawn orthogonal to the spine neck curvature. Spine head width was measured orthogonal to the axis of the spine neck. The length and width of each spine neck was determined by measuring the full width at half-maximum of a Gaussian fit applied to line profiles across the spine neck.

To evaluate the impact of nanoscale alterations in spine morphology on diffusional coupling, we calculated the compartmentalization factor, which is defined as:

$$CF = \frac{V * L}{A}$$

where V is the spine head volume, L the spine neck length and A the cross-sectional area of the spine neck. compartmentalization factor corresponds to the time constant τ of diffusional recovery ($\tau = \frac{V * L}{A * D}$) after a step change in concentration of a molecule with a diffusion coefficient D , serving as a quantitative measure of the degree of biochemical compartmentalization of a synapse⁴⁹.

Binding assays. On collection, the two hippocampi from each mouse were stored at -80°C . The hippocampi were then unfrozen in ice-cold Krebs solution (140 mM NaCl, 5 mM KCl, 25 mM HEPES, 1 mM EDTA, 10 mM glucose and pH 7.4) and sliced in a McIlwain chopper (800 μm). Each individual slice was then placed on a rubber surface, over a drop of ice-cold Krebs solution, and CA3 subslices were manually dissected under microscope magnification⁵⁰. To purify synaptic membranes, the CA3 subslices from each animal were placed in an eppendorf with 500 μl of ice-cold sucrose solution (0.32 M) containing 50 mM Tris-HCl, 2 mM EGTA and 1 mM dithiothreitol, pH 7.6, homogenized with a micro-Potter-Elvehjem and centrifuged at 3,000g for 10 min at 4°C . The supernatants were collected, centrifuged at 14,000g for 20 min at 4°C and the pellet was resuspended in 500 μl of a 45% (v/v) Percoll solution made up in a Krebs solution. After centrifugation at 14,000g for 2 min at 4°C , the top layer was removed (synaptosomal fraction), washed in 500 μl of Krebs solution and vigorously resuspended in 500 μl of Tris/Mg solution (50 mM Tris and 10 mM MgCl_2 , pH 7.4). The mixtures were centrifuged at 30,000g for 30 min to pull-down synaptic membranes and resuspended in 500 μl of Tris/Mg solution with 4 U ml^{-1} adenosine deaminase (Sigma), to remove endogenous adenosine. We have previously shown that the synaptic membranes provide an enrichment of markers of nerve terminals (SNAP-25, syntaxin-I) and of the postsynaptic density (PSD-95), which display a $<2\%$ contamination with astrocytic material, as gauged by the western blot evaluation of GFAP in the purified synaptosomes used to prepare synaptic membranes⁵¹.

To evaluate the binding density of $A_{2A}R$, we used ^3H -SCH58261 [2-(2-Furanyl)-7-(2-phenylethyl)-7H-pyrazolo[4,3-e][1,2,4]triazolo[1,5-c]pyrimidin-5-amine], which binds selectively cortical $A_{2A}R$ (ref. 52), whereas the binding density of A_1R was determined using ^3H -1,3-dipropyl-8-cyclopentylxanthine (DPCPX). Binding of ^3H -SCH58261 (specific activity of 77 Ci mmol^{-1} ; prepared by Amersham and generously offered by Dr Ennio Ongini, Shering-Plough, Milan, Italy) or of ^3H -DPCPX (specific activity of 102.1 Ci mmol^{-1} ; DuPont NEN, Boston, MA, USA) was for 2 h at room temperature with 6.5–13.5 $\mu\text{g ml}^{-1}$ of synaptosomal protein in a final volume of 200 μl in Tris/Mg solution containing 4 U ml^{-1} adenosine deaminase with a single supra-maximal and selective concentration of ^3H -DPCPX (10 nM) or of ^3H -SCH58261 (6 nM). Specific binding was determined by subtraction of the non-specific binding, which was measured in the presence of 1 μM 8-[4-[(2-aminoethyl)amino]carbonylmethyl-oxypheyl]xanthine (XAC), a mixed $A_1/A_{2A}R$ antagonist. Each binding assay data point was performed in duplicate. The binding reactions were stopped by vacuum filtration through glass fibre filters (B filters) using a 12-wells-Millipore harvester. The filters were then placed in scintillation vials and 4 ml of scintillation liquid cocktail (AquaSafe 500 Plus Ready Safe) was added. Radioactivity was determined after at least 12 h with a counting efficiency of 55–60% using a Tricarb 2900TR liquid scintillation analyser (Perkin Elmer). After subtraction of the non-specific from the total binding, the disintegration per min values corresponding to the specific binding were converted into absolute amounts fmol of bound ^3H -

SCH58261 or ^3H -DPCPX, which was normalized per mg of protein, quantified with the BCA method.

Behavioural experiments. The behavioural tasks, namely the modified Y-maze and object location tasks, were performed as a measurement of short-term spatial memory (to focus on CA3 region) and based on the innate preference of rodents to explore novelty. All the behavioural tests were performed during the light phase of the circadian cycle (between 08:30–02:00 hours), under red/low light (12lx). The intraperitoneal injection of SCH58261 was performed around 06:00 hours, to avoid the repercussion of the acute effect of the drug in the behavioural tasks and in the animal sleeping cycle. Between each trial the apparatus was cleaned with a 10% ethanol solution to avoid odour cues. At the end of the training trial, the mice were removed from the apparatus and kept in an individual cage during the inter-trial intervals. Mice were first tested in the object displacement test and then tested 12 h later in the modified Y-maze test, based on our previous validation that there is no influence of the object displacement test on the modified Y-maze test with this temporal interval either in control mice or in mice with memory deficits (Rial *et al.*⁵³). All experimental data was analysed using the ANY-maze video tracking system, Stoelting, US.

Modified Y-maze. The Y-maze apparatus consisted of three arms (42 cm long, 15 cm height and 8 cm large) made from impermeable black formica with a brown floor and was placed at the ground level. During the training phase, one arm was blocked by a removable door. In this phase the mice were positioned in the start arm, facing the center of the maze and allowed to explore only two arms (start and other) for 8 min. The test was performed 30 min later (with the door blocking the novel arm removed) and the animal were placed again in the start arm and allowed to explore the three arms during 8 min. The number of entries and the time spent in each arm was measured, as previously described^{53,54}.

Object displacement/object location. The object displacement protocol used was carried out as previously described^{53,54}. Briefly, the mice were first habituated for a 10-min period in the empty apparatus, a box composed by transparent plexiglass walls and brown floor (50 cm wide, 50 cm deep and 40 cm high), placed at the ground level. In the training phase, performed 24 h after the habituation phase, two identical plastic 50 ml Falcon tubes filled with dyed sterile water were placed 15 cm away from the walls of the arena. The mice were placed at the center of the apparatus and allowed to explore these two identical objects for 10 min, and we recorded the time spent sniffing/whisking or looking (≤ 1 cm) at the objects. The test was performed 30 min later, where one of the objects was moved creating a different spatial combination for the animal to explore during 5 min; again the time spent exploring the objects in the novel and familiar locations was recorded. All locations for the objects were counterbalanced among the groups. The displacement index was determined by the percentage of the time spent exploring the displaced object (T_{novel}) over the time spent exploring both objects. Displacement index is defined as $(T_{\text{novel}} \times 100) / (T_{\text{novel}} + T_{\text{familiar}})$.

SCH58261 injections (0.1 mg kg^{-1} , i.p.) were done each day, for 7 consecutive days before behavioural evaluation. Electrophysiological experiments were not carried out on animals used for behavioural experiments.

Statistical analysis. All statistical analyses were performed with Prism6 GraphPad Software. Values are presented as mean \pm s.e.m. in the text and figure legends. The data normality was tested using the D'Agostino & Pearson omnibus normality test. If data was normally distributed, a Student's *t*-test or one-way and two-way analysis of variance (ANOVA; to compare more than two independent groups) was performed; otherwise, a Mann-Whitney test was used (to compare two groups) and Kruskal-Wallis test followed by a Dunn's multiple comparison test (to compare more than two groups). Within-cell comparisons were made with Wilcoxon matched pairs test using non-normalized values. Data distributions were analysed using the Kolmogorov-Smirnov test with the data from wt mice as reference. Statistical differences were considered significant at $P < 0.05$.

Data availability. The data that support the findings of this study are available from the corresponding author on request.

References

- Sperling, R. Functional MRI studies of associative encoding in normal aging, mild cognitive impairment, and Alzheimer's disease. *Ann. N. Y. Acad. Sci.* **1097**, 146–155 (2007).
- Selkoe, D. J. Alzheimer's disease is a synaptic failure. *Science* **298**, 789–791 (2002).
- Kesner, R. P. A process analysis of the CA3 subregion of the hippocampus. *Front. Cell. Neurosci.* **7**, 78 (2013).
- Nakazawa, K. *et al.* Hippocampal CA3 NMDA receptors are crucial for memory acquisition of one-time experience. *Neuron* **38**, 305–315 (2003).
- Rolls, E. T. & Treves, A. The neuronal encoding of information in the brain. *Prog. Neurobiol.* **95**, 448–490 (2011).
- Marchetti, C. & Marie, H. Hippocampal synaptic plasticity in Alzheimer's disease: what have we learned so far from transgenic models? *Rev. Neurosci.* **22**, 373–402 (2011).

7. Sheng, M., Sabatini, B. L. & Südhof, T. C. Synapses and Alzheimer's disease. *Cold Spring Harb. Perspect. Biol.* **4** (2012).
8. Malinow, R. New developments on the role of NMDA receptors in Alzheimer's disease. *Curr. Opin. Neurobiol.* **22**, 559–563 (2012).
9. Ritchie, K. *et al.* The neuroprotective effects of caffeine: a prospective population study (the Three City Study). *Neurology* **69**, 536–545 (2007).
10. Cao, C. *et al.* High Blood caffeine levels in MCI linked to lack of progression to dementia. *J. Alzheimers Dis.* **30**, 559–572 (2012).
11. Dall'Igna, O. P. *et al.* Caffeine and adenosine A2a receptor antagonists prevent β -amyloid (25–35)-induced cognitive deficits in mice. *Exp. Neurol.* **203**, 241–245 (2007).
12. Li, P. *et al.* Optogenetic activation of intracellular adenosine A2A receptor signaling in the hippocampus is sufficient to trigger CREB phosphorylation and impair memory. *Mol. Psychiatry* **20**, 1339–1349 (2015).
13. Albasanz, J. L., Perez, S., Barrachina, M., Ferrer, I. & Martín, M. Up-regulation of adenosine receptors in the frontal cortex in Alzheimer's disease. *Brain Pathol.* **18**, 211–219 (2008).
14. Orr, A. G. *et al.* Astrocytic adenosine receptor A2A and Gs-coupled signaling regulate memory. *Nat. Neurosci.* **18**, 423–434 (2015).
15. Garcia-Alloza, M. *et al.* Characterization of amyloid deposition in the APPsw/PS1dE9 mouse model of Alzheimer disease. *Neurobiol. Dis.* **24**, 516–524 (2006).
16. Henze, D. A., Card, J. P., Barrionuevo, G. & Ben-Ari, Y. Large amplitude miniature excitatory postsynaptic currents in hippocampal CA3 pyramidal neurons are of mossy fiber origin. *J. Neurophysiol.* **77**, 1075–1086 (1997).
17. Debanne, D., Gähwiler, B. H. & Thompson, S. M. Long-term synaptic plasticity between pairs of individual CA3 pyramidal cells in rat hippocampal slice cultures. *J. Physiol. (Lond)* **507**(Pt 1): 237–247 (1998).
18. Wickersham, I. R., Finke, S., Conzelmann, K.-K. & Callaway, E. M. Retrograde neuronal tracing with a deletion-mutant rabies virus. *Nat. Methods* **4**, 47–49 (2006).
19. Tønnesen, J., Katona, G., Rózsa, B. & Nägerl, U. V. Spine neck plasticity regulates compartmentalization of synapses. *Nat. Neurosci.* **17**, 678–685 (2014).
20. Paoletti, P., Bellone, C. & Zhou, Q. NMDA receptor subunit diversity: impact on receptor properties, synaptic plasticity and disease. *Nat. Rev. Neurosci.* **14**, 383–400 (2013).
21. Hu, N.-W., Klyubin, I., Anwyl, R., Anwyl, R. & Rowan, M. J. GluN2B subunit-containing NMDA receptor antagonists prevent Abeta-mediated synaptic plasticity disruption *in vivo*. *Proc. Natl Acad. Sci. USA* **106**, 20504–20509 (2009).
22. Rönické, R. *et al.* Early neuronal dysfunction by amyloid β oligomers depends on activation of NR2B-containing NMDA receptors. *Neurobiol. Aging* **32**, 2219–2228 (2011).
23. Li, S. *et al.* Soluble A oligomers inhibit long-term potentiation through a mechanism involving excessive activation of extrasynaptic nr2b-containing nmda receptors. *J. Neurosci.* **31**, 6627–6638 (2011).
24. Talantova, M. *et al.* A β induces astrocytic glutamate release, extrasynaptic NMDA receptor activation, and synaptic loss. *Proc. Natl Acad. Sci. USA* **110**, E2518–E2527 (2013).
25. Papouin, T. *et al.* Synaptic and extrasynaptic NMDA receptors are gated by different endogenous coagonists. *Cell* **150**, 633–646 (2012).
26. Canas, P. M. *et al.* Adenosine A2A receptor blockade prevents synaptotoxicity and memory dysfunction caused by β -amyloid peptides via p38 mitogen-activated protein kinase pathway. *J. Neurosci.* **29**, 14741–14751 (2009).
27. Arendash, G. W. *et al.* Caffeine protects Alzheimer's mice against cognitive impairment and reduces brain β -amyloid production. *Neuroscience* **142**, 941–952 (2006).
28. Espinosa, J. *et al.* Caffeine consumption prevents memory impairment, neuronal damage, and adenosine A2A receptors upregulation in the hippocampus of a rat model of sporadic dementia. *J. Alzheimers Dis.* **34**, 509–518 (2013).
29. Tebano, M. T. *et al.* Adenosine A2A receptors and metabotropic glutamate 5 receptors are co-localized and functionally interact in the hippocampus: a possible key mechanism in the modulation of N-methyl-D-aspartate effects. *J. Neurochem.* **95**, 1188–1200 (2005).
30. Um, J. W. *et al.* Metabotropic glutamate receptor 5Is a Coreceptor for Alzheimer Ab oligomer bound to cellular prion protein. *Neuron* **79**, 887–902 (2013).
31. Trinchese, F. *et al.* Progressive age-related development of Alzheimer-like pathology in APP/PS1 mice. *Ann. Neurol.* **55**, 801–814 (2004).
32. Rebola, N., Carta, M., Lanore, F., Blanchet, C. & Mulle, C. NMDA receptor-dependent metaplasticity at hippocampal mossy fiber synapses. *Nat. Neurosci.* **14**, 691–693 (2011).
33. Barria, A. & Malinow, R. NMDA receptor subunit composition controls synaptic plasticity by regulating binding to CaMKII. *Neuron* **48**, 289–301 (2005).
34. Hanson, J. E., Pare, J.-F., Deng, L., Smith, Y. & Zhou, Q. Altered GluN2B NMDA receptor function and synaptic plasticity during early pathology in the PS2APP mouse model of Alzheimer's disease. *Neurobiol. Dis.* **74**, 254–262 (2015).
35. Schneider, L. S., Dagerman, K. S., Higgins, J. P. T. & McShane, R. Lack of evidence for the efficacy of memantine in mild Alzheimer disease. *Arch. Neurol.* **68**, 991–998 (2011).
36. Cunha, R. A. & Agostinho, P. M. Chronic caffeine consumption prevents memory disturbance in different animal models of memory decline. *J. Alzheimers Dis.* **20**(Suppl 1): S95–S116 (2010).
37. Zezula, J. & Freissmuth, M. The A2A-adenosine receptor: a GPCR with unique features? *Br. J. Pharmacol.* **153**(Suppl 1): S184–S190 (2008).
38. Dai, S. S. *et al.* Local glutamate level dictates adenosine A2A receptor regulation of neuroinflammation and traumatic brain injury. *J. Neurosci.* **30**, 5802–5810 (2010).
39. Rebola, N., Lujan, R., Cunha, R. A. & Mulle, C. Adenosine A2A receptors are essential for long-term potentiation of NMDA-EPSCs at hippocampal mossy fiber synapses. *Neuron* **57**, 121–134 (2008).
40. Yu, L. *et al.* Characterization of genomic organization of the adenosine A2A receptor gene by molecular and bioinformatics analyses. *Brain Res.* **1000**, 156–173 (2004).
41. Rombo, D. M. *et al.* Synaptic mechanisms of adenosine A2A receptor-mediated hyperexcitability in the hippocampus. *Hippocampus* **25**, 566–580 (2014).
42. de Almeida, L. P., Zala, D., Aebischer, P. & Déglon, N. Neuroprotective effect of a CNTF-Expressing lentiviral vector in the quinolinic acid rat model of Huntington's disease. *Neurobiol. Dis.* **8**, 433–446 (2001).
43. Gonçalves, N., Simões, A. T., Cunha, R. A. & de Almeida, L. P. Caffeine and adenosine A2A receptor inactivation decrease striatal neuropathology in a lentiviral-based model of Machado-Joseph disease. *Ann. Neurol.* **73**, 655–666 (2013).
44. Costenla, A. R. *et al.* Enhanced role of adenosine A2A receptors in the modulation of LTP in the rat hippocampus upon ageing. *Eur. J. Neurosci.* **34**, 12–21 (2011).
45. Rebola, N., Canas, P. M., Oliveira, C. R. & Cunha, R. A. Different synaptic and subsynaptic localization of adenosine A2A receptors in the hippocampus and striatum of the rat. *Neuroscience* **132**, 893–903 (2005).
46. Haberl, M. G. *et al.* An anterograde rabies virus vector for high-resolution large-scale reconstruction of 3D neuron morphology. *Brain Struct. Funct.* **220**, 1369–1379 (2015).
47. Bethge, P., Chéreau, R., Avignone, E., Marsicano, G. & Nägerl, U. V. Two-photon excitation STED microscopy in two colors in acute brain slices. *Biophys. J.* **104**, 778–785 (2013).
48. Tønnesen, J., Nadrigny, F., Willig, K. I., Wedlich-Söldner, R. & Nägerl, U. V. Two-Color STED microscopy of living synapses using a single laser-beam pair. *Biophys. J.* **101**, 2545–2552 (2011).
49. Wijetunge, L. S., Angibaud, J., Frick, A., Kind, P. C. & Nägerl, U. V. Stimulated emission depletion (STED) microscopy reveals nanoscale defects in the developmental trajectory of dendritic spine morphogenesis in a mouse model of fragile X syndrome. *J. Neurosci.* **34**, 6405–6412 (2014).
50. Cunha, R. A., Milusheva, E., Vizi, E. S., Ribeiro, J. A. & Sebastião, A. M. Excitatory and inhibitory effects of A1 and A2A adenosine receptor activation on the electrically evoked [3H]acetylcholine release from different areas of the rat hippocampus. *J. Neurochem.* **63**, 207–214 (1994).
51. Quiroz, C. *et al.* Key modulatory role of presynaptic adenosine A2A receptors in cortical neurotransmission to the striatal direct pathway. *Sci. World J.* **9**, 1321–1344 (2009).
52. Lopes, L. V. *et al.* Binding of the prototypical adenosine A2A receptor agonist CGS 21680 to the cerebral cortex of adenosine A1 and A2A receptor knockout mice. *Br. J. Pharmacol.* **141**, 1006–1014 (2004).
53. Rial, D. *et al.* Behavioral phenotyping of Parkin-deficient mice: looking for early preclinical features of Parkinson's disease. *PLoS ONE* **9**, e114216 (2014).
54. Kaster, M. P. *et al.* Caffeine acts through neuronal adenosine A2A receptors to prevent mood and memory dysfunction triggered by chronic stress. *Proc. Natl Acad. Sci. USA* **112**, 7833–7838 (2015).

Acknowledgements

This work was supported by the Centre National de la Recherche Scientifique, the Fundação para a Ciência e a Tecnologia, Santa Casa da Misericórdia, the Fondation France Alzheimer, the Agence Nationale de la Recherche (contract SynflAD), the Conseil Régional d'Aquitaine and the Labex Brain. Cellular imaging was in part performed at the Bordeaux Imaging Center, a service unit of the CNRS-INSERM and Bordeaux University, member of the national infrastructure France BioImaging. We thank Nelson Rebola and Mario Carta for their help with electrophysiology and their constant scientific support, Yoon Cho for her help with behavioural analysis and Melanie Ginger for the rabies virus.

Author contributions

S.V.S. and P.Z. performed the electrophysiology recordings. S.V.S. performed all the electrophysiology analysis. S.V.S. and M.G.H. performed all stereotaxic injections and subsequent immunolabellings. P.B. and V.N. performed STED acquisitions. P.B. and M.G.H. made the imaging analysis. C.L. and N.G. performed and analysed behaviour

experiments. A.G. performed immunostaining anti amyloid-beta plaques. F.Q.G. prepared synaptic membranes. C.B. provided help with electrophysiology analysis. R.A.C. performed binding assays and analysis, and helped with discussion. N.Go. produced shRNA and scrRNA lentiviral constructs and performed expression experiments. M.G.H. and A.F. provided rabies virus. C.M. provided supervision, guided the project and wrote the manuscript together with S.V.S. All authors discussed the results and commented on the manuscript.

Additional information

Supplementary Information accompanies this paper at <http://www.nature.com/naturecommunications>

Competing financial interests: the authors declare no competing financial interests.

Reprints and permission information is available online at <http://npg.nature.com/reprintsandpermissions/>

How to cite this article: Viana da Silva, S. *et al.* Early synaptic deficits in the APP/PS1 mouse model of Alzheimer's disease involve neuronal adenosine A_{2A} receptors. *Nat. Commun.* 7:11915 doi: 10.1038/ncomms11915 (2016).



This work is licensed under a Creative Commons Attribution 4.0 International License. The images or other third party material in this article are included in the article's Creative Commons license, unless indicated otherwise in the credit line; if the material is not included under the Creative Commons license, users will need to obtain permission from the license holder to reproduce the material. To view a copy of this license, visit <http://creativecommons.org/licenses/by/4.0/>